

Local dark matter clumps and the positron excess

Daniel Cumberbatch^{1*} and Joseph Silk^{1†}

¹*Department of Astrophysics, University of Oxford, Keble Road, Oxford OX1 3RH*

ABSTRACT

It has been proposed that the excess in cosmic ray positrons at approximately 8 GeV, observed on both flights of the HEAT balloon experiment, may be associated with the annihilation of dark matter within the Milky Way halo. In this paper we demonstrate how the self-annihilation of neutralino dark matter within local substructure can account for this excess, and estimate the annihilation cross-section for several benchmark minimal supersymmetric (MSSM) models. We also demonstrate the effect on the permitted parameter space as tidal stripping effects and destruction of substructure by mergers becomes increasingly severe.

Key words: Dark Matter

1 INTRODUCTION

A large body of evidence pertaining to the existence of non-baryonic cold dark matter (CDM) has been established over the past several decades, including the large-scale distribution of galaxies (Abazajian et al. (2003)), the study of primordial light element abundances (Cyburt et al. (2004)), galactic rotation curves (Begeman et al. (1991)), supernova data (Perlmutter et al. (1999)) and the power spectrum of anisotropies observed in the cosmic microwave background (CMB) (Bennett et al. (2003), de Bernardis et al. (2000)). At the 2σ confidence level, the CDM energy density parameter is now $\Omega_{\text{CDM}}h^2 = 0.113_{-0.018}^{+0.016}$ (Bennett et al. (2003)).

A popular candidate for CDM is the lightest supersymmetric (SUSY) neutralino, which is a superposition of Higgsinos, Winos and Binos. Consequently the neutralino is electrically neutral and colourless, only interacting weakly and gravitationally and therefore very difficult to detect directly. In R-parity conserving supersymmetric models the lightest neutralino, being the lightest SUSY particle (LSP), is stable (Weinberg et al. (2000)). Consequently, in a scenario where present-day CDM exists as a result of thermal-freeze out, the dominant species of CDM is likely to include the LSP. The relic density of the LSP will then heavily depend on its mass and annihilation cross-section. The neutralino is a popular candidate for CDM because the expected values of these parameters are such that the corresponding relic densities are of the same order as the currently accepted value of Ω_{CDM} .

In 1994 and 1995, the High-Energy Antimatter Telescope (HEAT) observed a flux in cosmic ray positrons, very much in excess of theoretical predictions, and peaking close to 8 GeV (Coutu et al. (1999)). This observa-

tion was confirmed by a second flight by HEAT in 2000 (Coutu et al. (2001)). The effect was originally predicted in 1984 (Silk et al. (1984)), for both cosmic ray positrons and antiprotons. While the cosmic ray antiproton feature remains elusive, at least for theorists it is now a well established idea that local dark matter annihilations are a possible source of the positrons contributing to the observed excess. Of course, improved data is urgently required to validate the significance of this observation, and these are expected to be taken in the near future by experiments like PAMELA, AMS-02 and Bess Polar. In this paper, we summarise why extant models for local dark matter annihilations fail to adequately account for the current spectral data on the positron feature, and present a new model.

Studies in which the local (within several kpc) distribution of dark matter is considered to be smooth have concluded that the dark matter annihilation rate is insufficient to reproduce the observed positron flux. This naturally leads to the idea of a non-uniform, or “clumpy”, dark matter distribution providing the overdensities necessary to elevate dark matter annihilation rates sufficiently to produce the observed excess (Baltz et al. (2001)). The distribution of such substructure can then be estimated through the use of simulations. Unfortunately, while simulations generally agree on the distribution of dark matter clumps, there is a divergence of opinion on the survival of the lightest clumps after the effects of hierarchical structure formation and tidal stripping are considered (Diemand et al. (2005), Zhao et al. (2005), Diemand et al. (2006)).

We note that throughout this paper we shall consider the LSP to be the lightest neutralino and therefore use the two terms synonymously.

* E-mail: dtc@astro.ox.ac.uk

† E-mail: silk@astro.ox.ac.uk

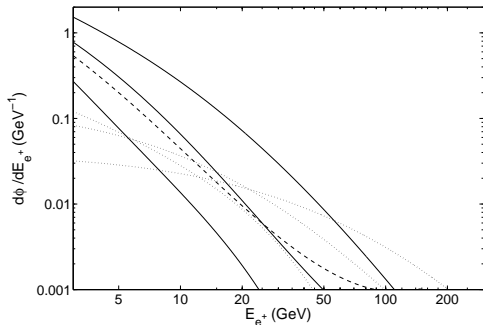


Figure 1. The positron energy spectra from neutralino annihilations for modes utilised in this paper. Solid lines represent the positron spectra, per annihilation, for $\chi\chi \rightarrow b\bar{b}$, for neutralinos with masses of 50, 150 and 600 GeV. Dotted lines are the same, but correspond to the process $\chi\chi \rightarrow \tau^+\tau^-$. Dashed lines correspond to the positron spectra from the process $\chi\chi \rightarrow W^+W^-$, for a 150 GeV neutralino, where the spectrum from the process $\chi\chi \rightarrow ZZ$ is very similar.

2 POSITRON SPECTRA FROM NEUTRALINO ANNIHILATION

Positrons can be produced in several neutralino annihilation modes. For example, monoenergetic positrons can result from the decay of gauge bosons produced in the processes $\chi\chi \rightarrow ZZ$ or $\chi\chi \rightarrow W^+W^-$, producing positrons of energy $m_\chi/2$, where m_χ is the neutralino mass. A small amount of positrons can result from the direct channel, $\chi\chi \rightarrow e^+e^-$, however such a channel seldom makes a significant impact on the overall positron flux. A continuum of positrons, extending to much lower energies, can also be produced in the cascades of particles produced in annihilations. The spectrum of positrons produced in neutralino annihilations can vary significantly depending on the mass and annihilation modes of the LSP.

If the neutralino is lighter than the W^\pm and Z bosons, annihilations will be dominated by the process $\chi\chi \rightarrow b\bar{b}$ with a minor contribution by $\chi\chi \rightarrow \tau^+\tau^-$. Assuming annihilations are dominated by the former process, the resulting positron spectrum will depend entirely on the mass of the LSP. For heavier LSPs, the annihilation products become more complex, often determined by several dominant annihilation modes including $\chi\chi \rightarrow W^+W^-$, $\chi\chi \rightarrow ZZ$ or $\chi\chi \rightarrow t\bar{t}$ as well as $\chi\chi \rightarrow b\bar{b}$ and $\chi\chi \rightarrow \tau^+\tau^-$. In our calculations, the positron spectrum per annihilation per energy interval $d\phi/dE_{e^+}$, uses results from PYTHIA (Sjostrand et al. (2001)), implemented in the DarkSUSY package (Gondolo et al. (2000)).

In figure 1, we display results for positron spectra from neutralino annihilations for the most important annihilation modes as produced by Hooper et al. (2004). Solid lines represent the positron spectrum, per annihilation, for $\chi\chi \rightarrow b\bar{b}$, for LSPs with masses of 50, 150 and 600 GeV. The dotted lines are the same, but from the process $\chi\chi \rightarrow \tau^+\tau^-$. Gaugino-like annihilations typically produce a spectrum which is dominated by $b\bar{b}$ at low energies, with contributions from $\tau^+\tau^-$ only becoming important at energies above about half the LSP mass. For neutralinos with a dominant higgsino component, annihilations to gauge bosons often

dominate. Dashed lines represent positron spectra resulting from the process $\chi\chi \rightarrow W^+W^-$ for a 150 GeV neutralino, where the spectrum corresponding to the process $\chi\chi \rightarrow ZZ$ is very similar.

3 POSITRON PROPAGATION MODEL

Cosmic ray positrons being electrically charged particles diffuse through the interstellar medium (ISM) under the electromagnetic influence of the galactic magnetic field and background radiation. The spatial distribution of the galactic magnetic field is extremely complex, resulting in positron trajectories which are well approximated to random walks. Whilst traversing the ISM, the positrons radiate through synchrotron losses owing, to the surrounding magnetic fields, and by inverse Compton scattering off of starlight and CMB background radiation (Webber et al. (1992)).

The diffusion-loss equation describing the above process is given by

$$\frac{\partial}{\partial t} \frac{\partial n_{e^+}}{\partial E_{e^+}} = \nabla \cdot \left[K(E_{e^+}, \mathbf{r}) \nabla \frac{\partial n_{e^+}}{\partial E_{e^+}} \right] + \frac{\partial}{\partial E_{e^+}} \left[b(E_{e^+}, \mathbf{r}) \frac{\partial n_{e^+}}{\partial E_{e^+}} \right] + Q(E_{e^+}, \mathbf{r}), \quad (1)$$

where $\partial n_{e^+}/\partial E_{e^+}$ is the number density of positrons per unit energy interval, $K(E_{e^+}, \mathbf{r})$ is a diffusion coefficient, $b(E_{e^+}, \mathbf{r})$ is the rate of energy loss and $Q(E_{e^+}, \mathbf{r})$ is the source term.

We parameterize the diffusion coefficient and the rate of energy loss as follows

$$K(E_{e^+}) = K_0(3^\alpha + E_{e^+}^\alpha) \approx 3 \times 10^{27} (3^{0.6} + E_{e^+}^{0.6}) \text{ cm}^2 \text{ s}^{-1} \quad (2)$$

and

$$b(E_{e^+}) = \tau_E E_{e^+}^2 \approx 10^{-16} E_{e^+}^2 \text{ s}^{-1}, \quad (3)$$

based upon measurements of stable nuclei in cosmic rays (primarily by fitting to observations of the boron to carbon ratio) (Maurin et al. (2002)), where in equations (2) and (3) we have assumed a spatially uniform galactic magnetic field. We then define K and b to be constant within a “diffusion zone”, which here is considered to be a radially-infinite cylindrical slab of thickness $2L \approx 4 \text{ kpc}$, which is the best-fit to observations (Maurin et al. (2002), Webber et al. (1992)).

We solve equation (1) for the local positron flux, using the procedure described in the appendix to this paper.

4 POSITRON AND ELECTRON BACKGROUNDS

In order to directly compare our results to the observations made by HEAT, we must calculate the ratio of the local positron flux to the combined local positron and electron fluxes, called the “positron fraction”. In order to do this we require the background spectra for secondary positrons, primary electrons and secondary electrons, where we propose that the primary positron component originates from the neutralino annihilations. In the following, we make use of the

parameterised fits to these spectra calculated by Edsjo et al. (1998) and stated here (in units of $\text{GeV}^{-1} \text{cm}^{-2} \text{s}^{-1} \text{sr}^{-1}$), as follows:

$$\left(\frac{d\Phi}{dE_{e^+}}\right)_{\text{prim. } e^-} = \frac{0.16\epsilon^{-1.1}}{1 + 11\epsilon^{0.9} + 3.2\epsilon^{2.15}} \quad (4)$$

$$\left(\frac{d\Phi}{dE_{e^+}}\right)_{\text{sec. } e^-} = \frac{0.70\epsilon^{0.7}}{1 + 110\epsilon^{1.5} + 600\epsilon^{2.9} + 580\epsilon^{4.2}} \quad (5)$$

$$\left(\frac{d\Phi}{dE_{e^+}}\right)_{\text{sec. } e^+} = \frac{4.5\epsilon^{0.7}}{1 + 650\epsilon^{2.3} + 1500\epsilon^{4.2}} \quad (6)$$

again where $\epsilon = E_{e^+}/(1 \text{ GeV})$. These equations agree with their respective observational results to within 10-15% for the relevant energy intervals. (For a more detailed account of the precision of these equations, refer to Strong et al. (2001).) The positron fraction is then calculated using

$$\frac{\left(\frac{d\Phi}{dE}\right)_{\text{prim. } e^+} + \left(\frac{d\Phi}{dE}\right)_{\text{sec. } e^+}}{\left(\frac{d\Phi}{dE}\right)_{\text{prim. } e^-} + \left(\frac{d\Phi}{dE}\right)_{\text{sec. } e^-} + \left(\frac{d\Phi}{dE}\right)_{\text{prim. } e^+} + \left(\frac{d\Phi}{dE}\right)_{\text{sec. } e^+}}. \quad (7)$$

5 DARK MATTER SUBSTRUCTURE

The standard cosmological model assumes that all structure in the universe originated from small amplitude quantum fluctuations during an epoch of inflationary expansion shortly after the big bang. The linear growth of the resulting density fluctuations is then completely determined by their initial power spectrum

$$P(k) = k^n, \quad (8)$$

where for $n \geq 1$, clumps are formed with a wide range of scales $\propto k^{-1}$. During the expansion of the universe, smaller clumps coalesce to form larger ones in a process of “bottom-up” hierarchical structure formation, in which the mass distribution at any given redshift can be determined through the use of numerical simulations.

In this paper we utilise the mass distribution of clumps deduced from the high-resolution simulations conducted by Diemand et al. (2005), of the form $dn_D/d\log(M/M_\odot) \propto (M/M_\odot)^{-1} \exp[-(M/M_{\text{cut-off}})^{-2/3}]$. Diemand et al. deduced a lower mass cut-off $M_{\text{cut-off}} \approx 8.03 \times 10^{-6} M_\odot$, however we shall also investigate the effect of using a much larger value, of order $10^6 M_\odot$ (similar to the typical mass resolution of conventional large-scale numerical simulations), to simulate the destruction of lighter clumps by merging. We normalise the distribution so that the number density of clumps between $10^{-6} M_\odot$ and $10^{-5} M_\odot$ is 500 pc^{-3} , with a halo-to-halo scatter factor of approximately 4, as stated by Diemand et al.. We also invoke an upper mass cut-off, $M_{\text{max}} \sim 10^{10} M_\odot$, defined so that heavier clumps possess a number density of less than 1 per unit volume within the region in which positrons contribute to the local flux.

The rate of dark matter annihilations within a clump crucially depends on its density profile. In this study we

adopt the widely used Navarro, Frenk & White (hereafter, NFW) density profile (Navarro, Frenk & White (1997))

$$\rho(r) = \frac{\rho_0}{c(r/r_{200})[1 + c(r/r_{200})]^2}, \quad (9)$$

which is consistent with simulated results for the outer regions large-scale halos. The NFW profile also provides a good fit to those of the lightest clumps produced in the simulations by Diemand et al. (Diemand et al. (2005)). The maximum radius of a clump is defined here to be the radius, r_{200} , at which its density is equal to 200 times the critical density. The concentration parameter c is a further degree of freedom, found to lie between $1.6 < c < 3$ for the clumps in Diemand et al.’s simulations. Since the relationship between clump mass and concentration is complex, we approximate that all clumps have the same concentration and we compare results when using $c = 1.6$ and 3.

Since the simulations conducted by Diemand et al. were terminated at $z = 26$, even though there is reason to believe that the shape of the mass distribution of clumps is similar today for large mass scales (Diemand et al. (2005)), we must also consider mass losses from tidal stripping by stars as clumps traverse the galactic halo. In this study we consider a scenario where the fractional mass loss experienced by each clump, over a given duration, is a mass-independent constant $1 - f$ and we compare results when using several different values of this parameter.

The notion of a universal tidal stripping parameter is consistent with the calculation by Zhao et al., who demonstrates that

$$\ln \frac{1}{f} \propto \frac{\langle \rho_* \rangle}{\rho_{\text{core}}^{1/2}} \Delta t, \quad (10)$$

where $\langle \rho_* \rangle$ is the average stellar density along the clump orbit, ρ_{core} is an effective “core” density of the clump and Δt is the time period considered. Since the majority of clumps have similar orbital parameters (Zhao et al. (2005)), and since we have adopted a universal clump profile, equation (10) implies that f is mass-independent.

6 POSITRON SPECTRA FROM DARK MATTER SUBSTRUCTURE

We consider four different neutralino models:

First, a 50 GeV neutralino with an annihilation branching ratio of 0.96 to $b\bar{b}$ and 0.04 to $\tau^+\tau^-$. Such a particle could be gaugino-like or higgsino-like, since for masses below the gauge boson masses, these modes dominate for either case (designated as model 1).

Second, we consider two cases for a 150 GeV neutralino. One which annihilates as described in model 1 (designated as model 2), and another which annihilates entirely to gauge bosons, W^+W^- or ZZ (designated as model 4). Such neutralinos are typically gaugino-like and higgsino-like respectively.

Finally we consider heavy, 600 GeV neutralinos, which annihilate to $b\bar{b}$ with a ratio of 0.87 and to $\tau^+\tau^-$ or t^+t^- the remaining time (designated as model 3). (We note that even though we do not explicitly calculate results for a model involving 600 GeV Higgsino-dominated neutralinos, which pri-

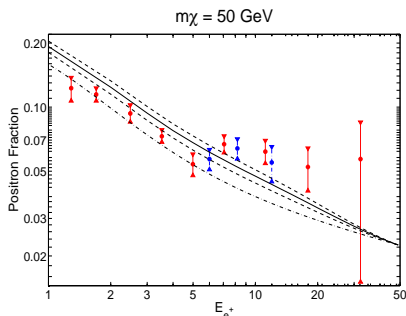


Figure 2. The calculated positron fraction as a function of positron energy (in GeV), for a 50 GeV neutralino which annihilates to $b\bar{b}$ 96% of the time and 4% to $\tau^+\tau^-$ (designated as model 1). The error bars displayed are for the 1994-95 (red) and 2000 (blue) HEAT data. The solid line represents the spectra which best fits the data. The best-fit χ^2 for this model is approximately 5.4, (for 12 data points). Dashed lines represent the spectra corresponding to the 1σ fits to the observations, where the normalisation of the positron flux was considered to be a free parameter. The dot-dashed line represents the non-exotic background contribution to the positron fraction.

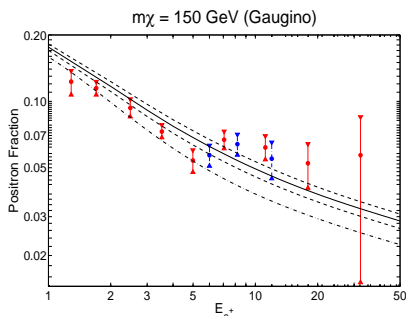


Figure 3. The calculated positron fraction as a function of positron energy (in GeV), for a 150 GeV neutralino which annihilates to $b\bar{b}$ 96% of the time and 4% to $\tau^+\tau^-$ (designated as model 2). The best-fit χ^2 for this model is 4.4, (for 12 data points). Otherwise, the same as in figure 2.

marily decay to gauge bosons and partially to Higgs bosons, the resulting positron spectra per annihilation is likely to be very similar to that of model 3).

Although these models do not fully encompass the extensive parameter space available to neutralinos at present, they do describe effective MSSM benchmarks. Furthermore, the relevant results for neutralinos with a mixture of the properties of those above can be inferred by interpolating between those presented.

Figures 2-5 display the positron fraction as a function of positron energy, calculated for each of the four MSSM models outlined above.

The thermally-averaged product of the low-velocity annihilation cross-section and relative speed of dark matter particles, $\langle\sigma v\rangle$, was left as a free parameter and varied to fit our results to observations. In each figure, the solid line displays the positron fraction which fitted best to 1σ error bars of the 94-95 (red) and 2000 (blue) HEAT data. Dashed lines correspond to positron fractions where χ^2 (for the 12 data points), differs by unity from the corresponding best-

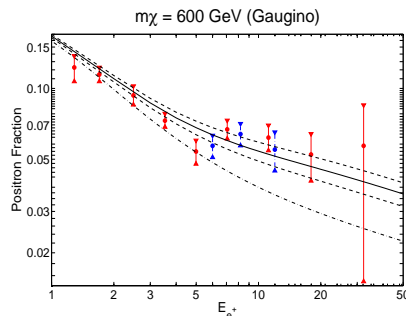


Figure 4. The calculated positron fraction as a function of positron energy (in GeV), for a 600 GeV neutralino which annihilates 87% to $b\bar{b}$ and 13% to $\tau^+\tau^-$ or t^+t^- (designated as model 3). The best-fit χ^2 for this model is 2.9, (for 12 data points). Otherwise, the same as in figure 2.

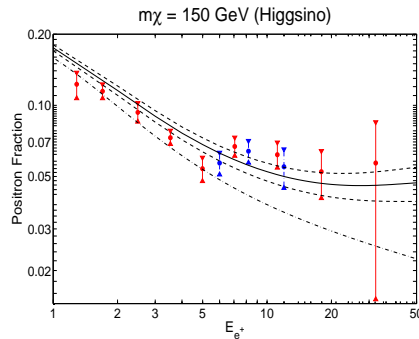


Figure 5. The calculated positron fraction as a function of positron energy (in GeV), for a 150 GeV neutralino which annihilates entirely to W^+W^- or Z^+Z^- (designated as model 4). The best-fit χ^2 for this model is 3.3, (for 12 data points). Otherwise, the same as in figure 2.

fit value (1σ results). Finally, the dot-dashed lines corresponds to the non-exotic background spectrum. The results are summarized in tables 1 and 2.

7 ASSESSMENT

The results displayed in figures 2-5 indicate that neutralino annihilations within local dark matter substructure can give rise to positron fractions which correspond well with observations, with χ^2 between 2.9 and 5.4, for values of $\langle\sigma v\rangle$ ranging from $10^{-29}\text{cm}^3\text{s}^{-1}$ for 50 GeV neutralinos to $2 \times 10^{-27}\text{cm}^3\text{s}^{-1}$ for 600 GeV neutralinos.

Such values of $\langle\sigma v\rangle$ are at least an order of magnitude smaller than the canonical estimate of $3 \times 10^{-26}\text{cm}^3\text{s}^{-1}$, determined from relic density calculations (Bertone et al. (2005)). However, many conventional MSSM models exist in which this approximation is grossly violated and are easily able to accommodate the results obtained, where the number of such models rapidly increases for lighter neutralinos, especially near 50 GeV (Hooper et al. (2005)).

As expected, we observe that the best-fit values of $\langle\sigma v\rangle$ increase as the dark matter clumps become increasingly stripped, and decrease as we increase their concentration, where the latter makes sense since a larger concentration

f	c=3		c=1.6	
	Best-Fit	$\frac{1\sigma}{10^{-29}}$	Best-Fit	$\frac{1\sigma}{10^{-29}}$
Model 1				
1.0	1.40	0.55-2.05	3.99	2.51-5.48
0.1	2.30	1.39-3.21	6.61	4.19-9.03
0.01	5.38	3.41-7.36	16.61	10.54-22.68
Model 2				
1.0	2.99	1.92-4.07	7.46	4.84-10.09
0.1	4.42	2.88-5.95	12.37	8.10-16.65
0.01	10.08	6.58-13.58	31.09	20.34-41.84
Model 3				
1.0	10.90	6.47-15.34	31.47	21.36-41.58
0.1	18.04	11.82-24.26	52.05	35.60-68.50
0.01	42.42	28.99-55.85	131.90	90.21-173.59
Model 4				
1.0	3.81	2.56-5.06	8.73	5.44-12.02
0.1	5.56	3.76-7.36	15.68	10.44-20.92
0.01	12.52	8.20-16.85	39.82	26.77-52.86

Table 1. Values of the product $\langle\sigma v\rangle$, in $\text{cm}^3 \text{s}^{-1}$, which give rise to positron fractions which best-fit the HEAT observations, for the four MSSM models considered, for $M_{\text{cut-off}} = 8.03 \times 10^{-6}$ and various values of c and f . One sigma error ranges are also displayed.

f	c=3		c=1.6	
	Best-Fit	$\frac{1\sigma}{10^{-29}}$	Best-Fit	$\frac{1\sigma}{10^{-29}}$
Model 1				
1.0	6.52	4.07-8.98	16.14	10.05-22.24
0.1	9.57	6.05-13.08	26.68	16.39-36.97
0.01	21.90	13.81-29.99	67.69	42.95-92.44
Model 2				
1.0	11.75	7.63-15.87	28.87	18.48-39.26
0.1	17.13	11.22-23.04	48.47	31.67-65.28
0.01	36.97	22.43-51.52	121.96	79.81-164.10
Model 3				
1.0	47.73	31.16-64.30	122.08	83.55-160.60
0.1	72.36	48.95-95.74	201.55	137.95-265.14
0.01	163.78	111.20-215.35	508.81	348.73-668.90
Model 4				
1.0	12.27	6.94-17.61	36.76	24.69-48.83
0.1	20.85	13.39-28.31	60.95	41.29-80.61
0.01	49.64	33.57-65.71	154.71	104.77-204.65

Table 2. Values of the product $\langle\sigma v\rangle$, in $\text{cm}^3 \text{s}^{-1}$, which give rise to positron fractions which best-fit the HEAT observations, for the four MSSM models considered, for $M_{\text{cut-off}} = 10^6$ and various values of c and f . One sigma error ranges are also displayed.

implies that an increasing proportion of the clump mass is contained within a smaller radius. However, we observe that even with up to 99% stripping, and varying the clump concentration over the entire range observed by Diemand et al., the best-fit values of $\langle\sigma v\rangle$ do not change by more than an order of magnitude.

We note that, of course, in reality the density of the clumps cannot diverge at their centres, as an NFW profile suggests, but are likely to possess uniformly dense cores containing of order 1% of their total mass (Zhao et al. (2005)). The stripping and eventual disintegration of these cores is a topic of much debate and is currently being investigated (Green et al. (2006)). We therefore do not display results for $f < 0.01$, since it is unknown as to whether these cores can survive such severe levels of disruption.

However, in table 2 we display results similar to those in table 1, now for $M_{\text{cut-off}} = 10^6 M_{\odot}$, corresponding to the typical mass resolution of simulations of the galactic halo, in order to simulate the destruction of lighter clumps. We observe that the best-fit values of $\langle\sigma v\rangle$ increase by no more than an order of magnitude compared to their corresponding values in table 1, but are more consistent with the canonical value and consequently consistent with a larger number of MSSM models.

We should also note that these results may be slightly modified when acknowledging flux contributions from tidal streams resulting from material stripped from clumps (Zhao et al. (2005)). However, owing to the significantly lower densities of these streams, compared to the clumps from which they originate, it is very likely that such effects will not significantly alter our results.

8 CONCLUSIONS

For each of the four benchmark supersymmetric models considered, we solved the diffusion-loss equation for the local positron flux resulting from neutralino annihilations within local dark matter substructures. We utilised the results from the unprecedentedly high resolution simulation conducted by Diemand et al., who determined that the lightest clumps to form are of order an Earth mass and as large as 10^{-2} pc. The mass distribution for clumps resulting from the simulation, which was terminated at $z = 26$, has been shown to be similar to be that expected today for large mass clumps. We assigned each clump an NFW density profile, with an associated universal concentration parameter consistent with the numerical results. We investigated the effects on the flux when invoking different degrees of (universal) mass loss suffered by each clump, in order to simulate the effects of tidal-stripping from stellar encounters.

Our results indicate that neutralino annihilations within local dark matter substructure can give rise to positron fractions which correspond well with the observations by HEAT, for values of $\langle\sigma v\rangle$ ranging from $10^{-29} \text{cm}^3 \text{s}^{-1}$ for 50 GeV neutralinos to $2 \times 10^{-27} \text{cm}^3 \text{s}^{-1}$ for 600 GeV neutralinos. Despite that such $\langle\sigma v\rangle$ are at least an order of magnitude smaller than the canonical value of $3 \times 10^{-26} \text{cm}^3 \text{s}^{-1}$, determined from relic density calculations we indicate that many conventional MSSM models exist in which this approximation is grossly violated and are easily able to accommodate our results obtained, where the number of such

models rapidly increases for lighter neutralinos, especially near 50 GeV.

We observed that even with up to 99% stripping, and varying the clump concentration over the entire range observed by Diemand et al., the best-fit values of $\langle\sigma v\rangle$ do not change by more than an order of magnitude. We also observed that even if we change the lower mass cut-off in our mass distribution from an Earth mass to 10^6 solar masses, the best-fit values of $\langle\sigma v\rangle$ increase by no more than an order of magnitude, but are consequently more consistent with a larger region of MSSM parameter space.

APPENDIX: DERIVATION OF THE STEADY-STATE POSITRON FLUX

Here we derive in detail the steady-state solution to the diffusion-loss equation (1), given by

$$\begin{aligned} \frac{\partial}{\partial t} \frac{\partial n_{e^+}}{\partial E_{e^+}} &= \nabla \cdot \left[K(E_{e^+}, \mathbf{r}) \nabla \frac{\partial n_{e^+}}{\partial E_{e^+}} \right] \\ &+ \frac{\partial}{\partial E_{e^+}} \left[b(E_{e^+}, \mathbf{r}) \frac{\partial n_{e^+}}{\partial E_{e^+}} \right] + Q(E_{e^+}, \mathbf{r}). \end{aligned} \quad (11)$$

Our treatment is very similar to that described in Edsjo et al. (1998), except that several unnecessary assumptions made in that derivation are omitted here, making our solution slightly more general.

We firstly re-arrange (11) in terms of the dimensionless parameter $u = 1/\epsilon = 1 \text{ GeV}/E_{e^+}$, and re-write the diffusion coefficient, given by (2), as $K = K_0 h(u)$, which gives

$$\frac{1}{h(u)} \frac{\partial}{\partial u} \frac{\partial n_{e^+}}{\partial u} = K_0 \tau_E \nabla^2 \frac{\partial n_{e^+}}{\partial u} - \tau_E [u^2 h(u)]^{-1} Q(\epsilon(u), \mathbf{r}), \quad (12)$$

where we have used equation (3) for the energy-loss rate, b . We now re-express (12) in terms of the variable v , where $h(u) = dv/du$. Provided that $h(u)$ is differentiable, we obtain

$$\frac{\partial}{\partial v} \frac{\partial n_{e^+}}{\partial u} = K_0 \tau_E \nabla^2 \frac{\partial n_{e^+}}{\partial u} - \tau_E [u^2 h(u)]^{-1} Q(\epsilon(v), \mathbf{r}). \quad (13)$$

Now making the substitutions

$$w(v) = -\frac{d\epsilon}{dv} = [u^2 h(u)]^{-1}, \quad (14)$$

and

$$F(v, \mathbf{r}) = \frac{\partial n_{e^+}(v, \mathbf{r})}{\partial u(v)}, \quad (15)$$

equation (13) becomes

$$\frac{\partial}{\partial v} F(v, \mathbf{r}) = K_0 \tau_E \nabla^2 F(v, \mathbf{r}) - \tau_E w(v) Q(\epsilon(v), \mathbf{r}). \quad (16)$$

As stated in Edsjo et al. (1998), equation (16) is analogous to an inhomogeneous heat equation. The spatial variables are exactly analogous, while v is analogous to "time". Since $v = \int h(u) du = 3^\alpha u + (1-\alpha)^{-1} u^{1-\alpha}$, we find that v is a monotonically increasing function for $\alpha < 1$, and therefore is appropriately analogised to time.

Considering the above, we can write the solution of the

steady-state positron number density as an integral over the effective source term, $-\tau_E w(v) Q(\epsilon(v), \mathbf{r})$, of equation (16), multiplied by a Green's function.

We firstly solve for the free Green's function G_{free} , which satisfies

$$\begin{aligned} \frac{\partial}{\partial v} G_{\text{free}}(v - v', \mathbf{r} - \mathbf{r}') &= K_0 \tau_E \nabla^2 G_{\text{free}}(v - v', \mathbf{r} - \mathbf{r}') \\ &= \delta(v - v') \delta(\mathbf{r} - \mathbf{r}'), \end{aligned} \quad (17)$$

which is identical to equation (16) with an effective source term $\delta(v - v') \delta(\mathbf{r} - \mathbf{r}')$, which is proportional to the source term for a monoenergetic point source, with $v = v'$, located at $\mathbf{r} = \mathbf{r}'$. Taking the (spatial) Fourier transform of (17), we obtain

$$\begin{aligned} \frac{\partial}{\partial v} \tilde{G}_{\text{free}}(v - v', \mathbf{k}) &+ K_0 \tau_E \nabla^2 k^2 \tilde{G}_{\text{free}}(v - v', \mathbf{k}) \\ &= (2\pi)^{-3/2} \delta(v - v') \exp(-i\mathbf{k} \cdot \mathbf{r}'), \end{aligned} \quad (18)$$

where \tilde{G}_{free} is the Fourier transform of G_{free} . Multiplying each side of (18) by the integrating factor $I = \exp(K_0 \tau_E k^2 v)$ and integrating over v , we obtain

$$\begin{aligned} \tilde{G}(v - v', \mathbf{k}) &= (2\pi)^{-3/2} \exp(-K_0 \tau_E k^2 (v - v')) \\ &\times \exp(-i\mathbf{k} \cdot \mathbf{r}') \theta(v - v'), \end{aligned} \quad (19)$$

where we have invoked the condition $G_{\text{free}} = 0$ (and therefore $\tilde{G}_{\text{free}} = 0$) for $v = 0$ (i.e. at infinite energy). Finally, we take the inverse Fourier transform of (19), to obtain

$$G_{\text{free}}(v - v', \mathbf{r} - \mathbf{r}') = (2\pi)^{-3/2} \int_{\mathbf{k}} \tilde{G}(v - v', \mathbf{k}) \exp(i\mathbf{k} \cdot \mathbf{r}) d^3 \mathbf{k}, \quad (20)$$

which evaluates to

$$G_{\text{free}}(v - v', \mathbf{r} - \mathbf{r}') = [D(v, v')]^{-3} \exp\left(\frac{(\mathbf{r} - \mathbf{r}')^2}{[D(v, v')]^2}\right), \quad (21)$$

where $D(v, v') = [4\pi K_0 \tau_E (v - v')]^{1/2}$.

As described in §3, our chosen diffusion zone is an infinite cylindrical slab of thickness $2L$, where positrons located outside of this region simply free-stream. Therefore the steady-state positron distribution must therefore vanish at $r = \infty$ and $|z| > L$. Ignoring contributions from sources outside of the diffusion zone, then from the form of the diffusion equation, the positron distribution will be zero for $|z| > L$ if it is zero at $z = \pm L$. Therefore in order to obtain our desired positron distribution within the diffusion zone, we can use a Green's function which simply vanishes at the boundaries of our diffusion zone. To do this we adopt the solution proposed by Edsjo et al. (1998), which utilises a set of image charges,

$$x'_n = x', \quad y'_n = y', \quad z'_n = 2Ln + (-1)^n z', \quad (22)$$

to find the required Green's function,

$$G_{2L}(v-v', \mathbf{r}-\mathbf{r}') = \sum_{n=-\infty}^{\infty} (-1)^n G_{\text{free}}(v-v', \mathbf{r}-\mathbf{r}'_n). \quad (23)$$

As described above, the steady-state positron distribution can then be expressed as the following integral

$$\begin{aligned} \frac{\partial n}{\partial \epsilon} &= \tau_E \epsilon^{-2} \int_0^{v(\epsilon)} dv' w(v') \\ &\times \int d^3 \mathbf{r}' G_{2L}(v(\epsilon)-v', \mathbf{r}-\mathbf{r}') Q(\epsilon(v'), \mathbf{r}'). \end{aligned} \quad (24)$$

Then using equation (14), we can conveniently re-express (24) as

$$\begin{aligned} \frac{\partial n}{\partial \epsilon} &= \tau_E \epsilon^{-2} \int_{\epsilon}^{\infty} d\epsilon' \\ &\times \int d^3 \mathbf{r}' G_{2L}(v(\epsilon)-v'(\epsilon'), \mathbf{r}-\mathbf{r}') Q(\epsilon, \mathbf{r}'). \end{aligned} \quad (25)$$

Now we must construct an appropriate source function, Q . To do this we only consider contributions from dark matter substructure, ignoring the contribution from the smooth component of the halo, which we calculate to be approximately 10^{-4} times the substructure component. As described in §4, we assume each clump to have an NFW profile, $\rho_{\text{NFW}}(c, r_{200}(M))$, with concentration, c , and maximum radius, $r_{200}(c, M)$, determined by c and the clump mass, M . The rate of production of positrons of energy ϵ GeV, is then

$$\frac{\langle \sigma v \rangle}{m_\chi^2} \frac{d\phi}{d\epsilon} \int_0^{r_{200}(c, M)} \rho^2(r') 4\pi r'^2 dr' = \frac{\langle \sigma v \rangle}{m_\chi^2} \frac{d\phi}{d\epsilon} f_{\text{NFW}}^2(c, M) \quad (26)$$

where $\langle \sigma v \rangle$ is the thermally-averaged, low-velocity annihilation cross-section multiplied by relative speed and $d\phi/d\epsilon$ is the number of positrons produced per annihilation per energy interval.

We must now multiply equation (26) by the correctly normalised density of clumps. As described in §4 we utilise the clump distribution, $dn_D(M)/d\log M$, determined by Diemand et al., normalised to a local clump density of 500 pc^{-3} , and like Diemand, we assume that this normalisation is proportional to the underlying halo density profile, ρ_{halo} . For simplicity, we choose the halo profile to be a 'cylindrically' symmetric NFW profile

$$\rho_{\text{halo}}(r) = \frac{\rho_0}{(r/R)(1+(r/R))^2} \quad (27)$$

where r is the cylindrical radial coordinate, $R \approx 20 \text{ kpc}$ and ρ_0 is a constant. The correctly normalised, spatially-dependent mass distribution of clumps is then

$$\begin{aligned} \frac{dn(r, M)}{d\log M} &= \frac{\rho_{\text{halo}}(r)}{\rho_{\text{halo}}(r=R_\odot)} \frac{dn_D(M)}{d\log M} \\ &\simeq \frac{0.86}{(r/R)(1+(r/R))^2} \frac{dn_D(M)}{d\log M}, \end{aligned} \quad (28)$$

where $R_\odot \approx 8.5 \text{ kpc}$, is the approximate distance between the Earth and the galactic centre.

Considering the above, the source function is given by

$$Q(\epsilon, r) = \frac{\langle \sigma v \rangle}{m_\chi^2} \frac{d\phi}{d\epsilon} \int_{M_{\text{min}}}^{M_{\text{max}}} f_{\text{NFW}}^2(c, M) \frac{dn_D(M)}{d\log M} d\log M, \quad (29)$$

where $M_{\text{min}} \sim 10^{-6} M_\odot$ and $M_{\text{max}} \sim 10^{10} M_\odot$, as discussed in §4.

Substituting expressions (23), (29) and (28) into equation (25), evaluated at $z=0$ and $r=R_\odot$, we obtain the required (local) positron number density

$$\begin{aligned} \left(\frac{\partial n_{e^+}}{\partial \epsilon} \right)_{\text{local}} &= \frac{\langle \sigma v \rangle \tau_E}{(m_\chi \epsilon)^2} \int_{M_{\text{min}}}^{M_{\text{max}}} f_{\text{NFW}}^2(c, M) \frac{dn_D(M)}{d\log M} d\log M \\ &\times \int_{\epsilon}^{\infty} d\epsilon' \{D[v(\epsilon), v'(\epsilon')]\}^{-3} \frac{d\phi}{d\epsilon'} \sum_{n=-\infty}^{\infty} (-1)^n \\ &\times \int_{-L}^L dz' \exp \left[- \left(\frac{(-1)^n z' + 2Ln}{D[v(\epsilon), v'(\epsilon')]} \right)^2 \right] \\ &\times \int_0^{\infty} dr' r' \frac{0.86}{(r'/R)(1+(r'/R))^2} \\ &\times \exp \left(- \frac{R_\odot^2 + r'^2}{\{D[v(\epsilon), v'(\epsilon')]\}^2} \right) \\ &\times \int_0^{2\pi} d\theta' \exp \left(\frac{2rr' \cos \theta'}{\{D[v(\epsilon), v'(\epsilon')]\}^2} \right). \end{aligned} \quad (30)$$

The θ' integral evaluates to $2\pi I_0$, where I_0 is a modified Bessel function of the first kind and the z' integral evaluates to the following sum of error functions,

$$\begin{aligned} H(L, D) &= \pi^{1/2} D \left(\text{erf} \left(\frac{L}{D} \right) + \sum_{m=1}^{\infty} \left\{ \text{erf} \left[\frac{(4m-3)L}{D} \right] \right. \right. \\ &\left. \left. + \text{erf} \left[\frac{(4m+1)L}{D} \right] - 2 \text{erf} \left[\frac{(4m-1)L}{D} \right] \right\} \right) \end{aligned} \quad (31)$$

We are then left with integrals over ϵ' and r' ,

$$\begin{aligned} \left(\frac{\partial n_{e^+}}{\partial \epsilon} \right)_{\text{local}} &= \frac{2R \langle \sigma v \rangle \tau_E}{(m_\chi \epsilon)^2} \int_{M_{\text{min}}}^{M_{\text{max}}} f_{\text{NFW}}^2(c, M) \frac{dn_D(M)}{d\log M} d\log M \\ &\times \int_{\epsilon}^{\infty} d\epsilon' [D(v, v')]^{-2} \frac{d\phi}{d\epsilon'} H(L, D(v, v')) \\ &\times \int_0^{\infty} dr' \frac{0.86}{(1+(r'/R))^2} \\ &\times \exp \left(- \frac{R_\odot^2 + r'^2}{[D(v, v')]^2} \right) \\ &\times I_0 \left(\frac{2R_\odot r'}{[D(v, v')]^2} \right), \end{aligned} \quad (32)$$

which we evaluate numerically.

Finally, using equation (32), we obtain the local positron flux resulting from neutralino annihilations to be

$$\left(\frac{d\Phi_{e^+}}{d\epsilon}\right)_{\text{local}} = \frac{\beta c}{4\pi} \left(\frac{dn_{e^+}}{d\epsilon}\right)_{\text{local}}, \quad (33)$$

where βc is the speed of a positron of energy ϵ .

ACKNOWLEDGEMENTS

We would like to thank S. Nussinov and D. Hooper for various discussions with us on this topic.

REFERENCES

- Abazajian K. *et al.* [SDSS Collaboration] astro-ph/0305492; Bergman K. G., Broeils A. H., Sanders R. H. 1991 MNRAS, 249, 523; Davis M., Efstathiou G., Frenk C. S. & White S. D. 1985 ApJ, 292, 371
- Baltz E. A., Edsjo J., Freesea K., Gondolo P., 2001, (astro-ph/0109318)
- Begeman K. G., Broeils A. H., Sanders R. H., 1991, MNRAS, 249, 523
- Bennett C. L., 2003, (astro-ph/0302207)
- Bertone G., Hooper D., Silk J., 2005, Phys. Rep., 405, 5
- Coutu S. *et al.*, Astropart. Phys. **11**, 429 (1999)
- Coutu S. *et al.* [HEAT-pbar Collaboration], "Positron measurements with the HEAT-pbar instrument", Proceedings of 27th ICRC (2001).
- Cyburt R. H., 2004, Phys. Rev. D, 70, 023505 (astro-ph/0401091)
- de Bernardis P. *et al.* 2000 Nature **404**, 955 (astro-ph/0004404); Hanany S. *et al.* 2000 ApJ, 545, L5 (astro-ph/0005123); Balbi A. *et al.*, 2000 ApJ, 545, L1 [Erratum-ibid. **558**, L145 (2001)]; Netterfield *et al.* C. B. [Boomerang Collaboration], 2002 ApJ, 571, 604 Broeils A. H., Sanders R. H. (1991) MNRAS, 249, 523; Davis M., Efstathiou G., Frenk C. S. & White S. D. (1985) ApJ, 292, 371
- Diemand J., Moore B., Stadel J., 2005, Nature **433**, 389
- Diemand J., Kuhlen M., Madau P., 2006, astro-ph/0603250
- Edsjo J., Baltz E., 1998, (astro-ph/9808243)
- Gondolo P., Edsjo J., Bergstrom L., Ullio P., Baltz E. 2000, (astro-ph/0012234)
- Green A.M., Goodwin S.P., 2006, astro-ph/0604142
- Hooper D., Taylor J., Silk J., 2004, (arXiv:hep-ph/0312076)
- Hooper D., Silk J., 2005, Phys. Rev. D, 71, 083503 (hep-ph/0409104)
- Maurin D., Donato F., Taillet R., Salati P., 2002, A&A, 394, 1039 (astro-ph/0206286)
- Navarro J.F., Frenk C.S., White S.D.M., 2006, ApJ, 490, 493
- Perlmutter S. *et al.* [Supernova Cosmology Project Collaboration] 1999, ApJ, 517, 565 (astro-ph/9812133)
- Silk J., Srednicki M., 1984, Physical Review Letters, 53, 624
- Sjostrand T., Eden P., Friberg C., Lonnblad L., Miu G., Mrenna S., Norrbin E., 2001, Comput. Phys. Commun. **135**, 238 (arXiv:hep-ph/0010017)
- Strong A. W., Moskalenko I. V., 2001, (astro-ph/0101068)
- Webber W. R., Lee M. A., Gupta M., 1992, ApJ, 390, 96
- Weinberg S. 1982 Phys. Rev. D, 26, 287; Hall L. J. & Suzuki M. 1984 Nucl. Phys. B **231**, 419; Alanach B. C., Dedes A., & Dreiner H. K., 1999 Phys. Rev. D, 60, 075014
- Zhao H., Taylor J. E., Silk J., Hooper D., 2005, (astro-ph/0508215)